Time-reversal techniques for MISO and MIMO wireless communication systems

Ahmed E. Fouda,[1] Fernando L. Teixeira,[1] and Mehmet E. Yavuz[2]

Received 12 March 2012; revised 26 July 2012; accepted 8 September 2012; published 20 October 2012.

[1] We consider the application of different time-reversal (TR) signal processing and beamforming techniques to multiple-input single-output (MISO) and multiple-input multiple-output (MIMO) wireless communication systems. Conventional TR beamforming provides spatial focusing at the intended receiver; however, it does not yield perfect channel equalization. Time-reversed pilot can be normalized to provide perfect equalization at the expense of power level. This equalization is particularly important for high data rates where the bit error rate performance is dominated by internal noise due to intersymbol interference. To increase physical layer covertness, TR beamforming is combined with the multiple-signal-classification (MUSIC) technique to produce null fields at eavesdroppers. This technique is also applied to MIMO setups to eliminate interuser interference and hence increase system capacity. Differential TR is used to obtain and update pilot signals for passive moving receivers, i.e., those that cannot (or do not) transmit pilot signals. Time-reversed differential backscattered signal is able to provide satisfactory spatial and temporal focusing at the moving receiver.

Citation: Fouda, A. E., F. L. Teixeira, and M. E. Yavuz (2012), Time-reversal techniques for MISO and MIMO wireless communication systems, *Radio Sci.*, *47*, RS0P02, doi:10.1029/2012RS005013.

1. Introduction

[2] With the continuous increase in demand for higher data rates in wireless communications, ultrawideband (UWB) systems are becoming more popular [*Siwiak*, 2002]. Despite their advantages, UWB systems are very sensitive to delay spreads caused by multipath in rich scattering environments and require complex and expensive receivers to compensate for delays of different replicas of the desired received signal. The application of time-reversal (TR) techniques to UWB wireless communication and radar systems has gained increasing interest recently [*Derode et al.*, 2003; *Lerosey et al.*, 2005; *Kyritsi et al.*, 2004; *Nguyen et al.*, 2005, 2006a; *Guo et al.*, 2007; *Wang and Lv*, 2011; *Kaiser and Zheng*, 2010; *Jin et al.*, 2010]. TR provides a simple and cost-efficient solution to the problem of delay spread in UWB systems. It moves the burden of equalization from the receiver side to the transmitter and channel sides, thus allowing for simpler and cheaper receivers at the expense of some added complexity to the transmitter [*Guo et al.*, 2007].

[3] TR provides both temporal and spatial focusing of the signal at the receiver [*Edelmann et al.*, 2005; *Lerosey et al.*, 2004]. Not only does it mitigate negative effects of multipath, but also it is capable of actually harnessing multipath to achieve better focusing resolution (super-resolution) both in time and space [*Lerosey et al.*, 2004; *Derode et al.*, 2003; *Lerosey et al.*, 2005; *Montaldo et al.*, 2004; *Yavuz and Teixeira*, 2005]. The temporal focusing property amounts to a type of pre-equalization procedure that reduces (or cancels) intersymbol interference (ISI) at the receiver [*Blomgren et al.*, 2008]. Spatial focusing combats channel fading [*Edelmann et al.*, 2005], maximizes delivered power to the intended receiver, and therefore enables power saving at the transmitter side and/or increasing channel capacity and communication range. Spatial focusing also reduces power leakage to other locations. This is very important to reduce interuser interference (IUI) in multiuser configurations, which in turn allows for a more effective use of space-division multiple access (SDMA) to boost the system capacity [*Nguyen et al.*, 2005; *Wang and Lv*, 2011; *Kaiser and Zheng*, 2010; *Naqvi and Zein*, 2011]. Spatial focusing also adds a degree of physical layer security (covertness) to the systems, making it hard for eavesdroppers away from the intended receiver's location to decode the signal using traditional decoding techniques [*Blomgren et al.*, 2008; *Li et al.*, 2009].

[4] In this paper, we study the application of different TR techniques to wireless communication systems. We start with a brief review on the basics of TR communication and its performance metrics. Then, we consider multiple-input single-output (MISO) configurations, where there exists one intended receiver and possibly one or more eavesdroppers. We introduce and study the applicability of three TR techniques, namely, (1) equalized TR beamforming, (2) TR beamforming with multiple-signal-classification (MUSIC),

[1]ElectroScience Laboratory, Department of Electrical and Computer Engineering, Ohio State University, Columbus, Ohio, USA.
[2]Intel Corporation, Hillsboro, Oregon, USA.

Corresponding author: A. E. Fouda, ElectroScience Laboratory, Department of Electrical and Computer Engineering, Ohio State University, 1330 Kinnear Rd., Columbus, OH 43212, USA. (fouda.1@osu.edu)

0048-6604/12/2012RS005013

and (3) differential TR, in both free-space and rich scattering environments. Equalized TR beamforming yields perfect channel equalization on the expense of spatial focusing. TR beamforming combined with MUSIC produces null fields at eavesdroppers locations for increased physical layer covertness. Differential TR is used to extract the pilot signal of passive moving receivers (scatterers) from array acquisitions [*Fouda and Teixeira*, 2012]. These passive receivers may represent, for example, receivers in one-way communication links, sensors such as passive RFIDs or intercepting eavesdroppers. We highlight relative strengths and limitations of these different techniques, and compare their bit error rate performances under high and low data rates operations. We also compare the performance of equalized TR beamforming in rich scattering scenarios with that of conventional (non-equalized) TR and conventional (non TR-based) beamforming. Finally, we consider multiple-input multiple-output (MIMO) configurations, where TR beamforming with MUSIC is shown to significantly reduce undesired interuser interference.

2. Time-Reversal Communications and Performance Metrics

[5] Consider a MISO communication link between an N elements transmitter array and a receiver (let us call it receiver A). In TR-based communication systems, to start the link, the receiver transmits a signal that is recorded by the transmitter array elements. These recorded N signals constitute the steering vector (column vector of Green's functions or equivalently impulse responses) between receiver A and each element in the array. The steering vector (or processed versions of it, as discussed later) is used as a pilot for information signal transmission from the array to receiver A. From the time-reversal invariance of the wave equation, when the N signals of the pilot are time-reversed and simultaneously transmitted, they tend to automatically focus at the intended receiver location (regardless of the intervening medium which is, in general, not known to the transmitter array) and produce a compressed pulse in time as well [*Lerosey et al.*, 2005; *Derode et al.*, 2003]. After time-reversed back-propagation, the received signal, in the frequency domain, at location i is given by the following inner product

$$H_i(\omega) = \langle \mathbf{g}_i(\omega), \mathbf{p}_A(\omega) \rangle \tag{1}$$

where $\mathbf{p}_A(\omega)$ is the pilot vector of receiver A, $\mathbf{g}_i(\omega) = [G_{(i,1)}(\omega),.., G_{(i,N)}(\omega)]^T$ is the steering vector of location i, where $G_{(i,n)}(\omega)$ is the Green's function between location i and the nth element of the array, and $\langle \mathbf{a}, \mathbf{b} \rangle = \mathbf{b}^\dagger \mathbf{a}$ denotes the inner product between $\mathbf{a}$ and $\mathbf{b}$ where † represents a conjugate transpose.

[6] The received signal in the time domain is obtained by taking the inverse Fourier transformation $h_i(t) = \mathscr{F}^{-1}\{H_i(\omega)\}$. We refer to $h_i(t)$ as the equivalent channel impulse response after TR, or simply the channel impulse response (CIR). The CIR peak at location i is defined as $\eta_i = \max_t |h_i(t)|$. This will be used as a measure for the spatial distribution of energy [*Oestges et al.*, 2004].

[7] The intersymbol interference (ISI) is defined as the ratio of the sum of values of the CIR, offset by integer multiples of T from the peak, to the peak value of CIR [*Fouque et al.*, 2007], as follows

$$ISI_i = \frac{\sum_{n=-N_1, n\neq 0}^{N_2} |h_i(\overline{\tau_i} + nT)|}{|h_i(\overline{\tau_i})|} \tag{2}$$

where T is the symbol duration, $\overline{\tau_i}$ is the time delay of the CIR peak at location i, $N_1 = \lfloor \overline{\tau_i}/T \rfloor$, and $N_2 = \lfloor (\tau - \overline{\tau_i})/T \rfloor$, where τ is the duration of the CIR.

[8] An information signal $s(t)$ is convolved with the time-reversed pilots. The transmitted signal vector intended for receiver A is given by $\mathbf{t}_A(t) = s(t) *_t \mathbf{p}_A(-t)$, where $*_t$ denotes convolution. The received signal can be written as $r_A(t) = s(t) *_t h_A(t) + n(t)$, where $n(t)$ is the additive noise at the receiver.

3. TR Techniques for Wireless Communications

[9] In this section, the *exact* steering vector of the receiver, also known as the channel state information (CSI) between the array and the receiver, is assumed to be perfectly known to the transmitters. This implies that the time period that the transmitter array takes to record the receiver's steering vector is long enough to capture (mostly) all the multiple scattering in the medium. In addition, the sampling rate is equal to or higher than the Nyquist sampling rate corresponding to the bandwidth of operation. In other words, we are assuming that TR does not add intrinsic bandwidth limitation, i.e. if the original communication system (before using TR) is capable of generating signals with certain bandwidth B, we assume that it will also be capable of generating and sampling the TR pilot over the same bandwidth. Deviations from ideality due to some hardware limitations are discussed in section 4.4.

3.1. TR Beamforming

3.1.1. Conventional TR (Without Equalization)

[10] The simplest form of the pilot is to coincide with the steering vector of the intended receiver [*Kyritsi et al.*, 2004], that is

$$\mathbf{p}_A(\omega) = \mathbf{g}_A(\omega) \tag{3}$$

This choice exhibits high spatial focusing performance that is further enhanced in rich scattering scenarios, as will be shown in the next section. However, the equivalent CIR at the intended receiver is proportional to $\|\mathbf{g}_A(\omega)\|^2$, where $\|\mathbf{g}_A(\omega)\|$ is the norm of $\mathbf{g}_A$ given by $\|\mathbf{g}_A\| = \sqrt{\langle \mathbf{g}_A, \mathbf{g}_A \rangle}$. This means that the CIR is not flat with frequency, i.e. the equivalent channel transfer function is not perfectly equalized. This gives rise to undesired intersymbol interference which hampers performance in case of high data rates.

3.1.2. Equalized TR

[11] In order to achieve perfect equalization at the receiver, the steering vector can be normalized by the square of its norm as follows

$$\mathbf{p}_A(\omega) = \frac{\mathbf{g}_A(\omega)}{\|\mathbf{g}_A(\omega)\|^2} \tag{4}$$

This guarantees a flat CIR at the receiver, as can be easily deduced from (1). This choice, however, implies inferior spatial focusing performance as compared with conventional TR, as shown later. We note that temporal side lobes suppression by iterative TR [*Montaldo et al.*, 2004] and spatial linear inversion based on TR [*Lemoult et al.*, 2009] are interesting techniques which do not require any inversion, and are probably less sensitive to noise. However, these techniques require precise weighting of the gain factors in each iteration to guarantee convergence. Also, they require extra processing at the user to subtract, time-reverse, and transmit the differential signal in each iteration, rather than sending the user's pilot only once at the beginning.

[12] It is interesting to contrast TR techniques with the waterfilling power allocation scheme in which the transmitter allocates more power to stronger sub-carriers, and less or even no power to weaker ones [*Tse and Viswanath*, 2005]. In that case, the goal is to maximize the signal to (external) noise ratio at the receiver, regardless of the equalization of the received signal or ISI. This is analogous to what conventional TR (or a matched filter) does. On the other hand, equalized TR basically does the reverse: the gain assigned to each frequency is inversely proportional to the channel response at that frequency, as described in (4). The goal here is to have equalized (flat) channel response at the receiver after backpropagation.

3.2. Conventional Beamforming

[13] In conventional (non TR-based) beamforming, the information available to the array about the receiver can be its direction (which can be estimated using some direction of arrival (DOA) algorithms [*Gross*, 2005]), or, in the best-case scenario, its position with respect to the array. So if we assume that the array knows the receiver location, it can generate an approximate pilot, which is the steering vector of the receiver location based on free-space assumption. Note that although the array may know the receiver's location, it does not know its exact CSI. Following the above discussion, the pilot vector of conventional beamforming can be written as

$$\mathbf{p}_A(\omega) = \frac{\widetilde{\mathbf{g}}_A(\omega)}{\|\widetilde{\mathbf{g}}_A(\omega)\|^2} \tag{5}$$

where $\widetilde{\mathbf{g}}_A$ is the steering vector of receiver A based on some background medium assumption that may not correspond to the actual one.

3.3. TR Beamforming With Nulling at Eavesdroppers

[14] If one of the concerns of the communication system is to minimize information leakage to eavesdroppers (or interuser interference in case of MIMO configurations), TR beamforming can be combined with MUSIC algorithm to produce null fields at eavesdroppers. Assume the presence of M eavesdroppers $M < N$, whose steering vectors are known to the array. The pilot of receiver A can be orthogonalized to each and everyone of the steering vectors of the M eavesdroppers as follows

$$\mathbf{p}_A(\omega) = \frac{\mathbf{g}_A(\omega)}{\|\mathbf{g}_A(\omega)\|^2} - \sum_{i=1}^{M} \left\langle \frac{\mathbf{g}_A(\omega)}{\|\mathbf{g}_A(\omega)\|^2}, \hat{\mathbf{g}}_i(\omega) \right\rangle \hat{\mathbf{g}}_i(\omega) \tag{6}$$

where

$$\hat{\mathbf{g}}_i(\omega) = \frac{\mathbf{g}_i(\omega)}{\|\mathbf{g}_i(\omega)\|} \tag{7}$$

For the above processing to produce ideal nulling at the M locations, the M steering vectors ($\mathbf{g}_i(\omega)$, $i = 1,., M$) must be mutually orthogonal. The pilot given by (6) does not produce perfectly equalized CIR at the intended receiver. For perfect equalization, the pilot is normalized as follows

$$\overline{\mathbf{p}}_A(\omega) = \frac{\mathbf{p}_A(\omega)}{\langle \mathbf{g}_A(\omega), \mathbf{p}_A(\omega) \rangle^*} \tag{8}$$

3.4. Extracting Pilot Signals Using Differential TR

[15] For scenarios involving receivers that are unable to transmit pilots, like, for example, passive RFIDs or receivers in one-way communication links, differential TR techniques [*Fouda and Teixeira*, 2012] can be used to extract an approximate version of the receiver's pilot. Assuming that the initial location of the receiver (denoted by location 0) is known to the array, differential TR proceeds as following: the array transmits a beam $\mathbf{g}_0(\omega)$ twice at two close time instants. The beam illuminates the moving receiver (target) at two adjacent locations (locations 1 and 2), and backscatterings from both illuminations ($\mathbf{s}_1(\omega)$ and $\mathbf{s}_2(\omega)$) are recorded and subtracted to yield the differential backscattering vector, written as $\mathbf{d}(\omega) = \mathbf{s}_2(\omega) - \mathbf{s}_1(\omega)$. It was shown in *Fouda and Teixeira* [2012] that when $\mathbf{d}(\omega)$ is time-reversed and backpropagated, it focuses in the vicinity of the moving target. Therefore, $\mathbf{d}(\omega)$ can be used as a pilot for communication. To achieve better equalization at the receiver, $\mathbf{d}(\omega)$ can be normalized as follows

$$\mathbf{p}_A(\omega) = \frac{\mathbf{d}(\omega)}{\langle \mathbf{g}_0(\omega), \mathbf{d}(\omega) \rangle^*} \tag{9}$$

4. MISO Configuration

4.1. Problem Setup

[16] In this section, we assess and contrast the performances of the proposed TR techniques applied to MISO configurations. MISO here refers to the configuration where a multiple-input antenna array is communicating with one single intended receiver. To assess the covertness property offered by TR, we assume the presence of one eavesdropper, and compare the performance of the wireless channel at both the intended receiver and the eavesdropper. Our goal is to maximize the signal "quality" at the receiver, while achieving maximum covertness (low probability of intercept (LPI)) at the eavesdropper [*Blomgren et al.*, 2008].

[17] The simulation domain is either extended free-space or a 3.6 m × 3.6 m room surrounded by 60 cm thick walls with relative permittivity of 4. The transceiver array consists of eight point sources in 2-D. The simulation is therefore a 2-D domain with electric field transverse to the domain (scalar case). Two array deployments are considered: (1) a dense linear array with inter-element spacing of 15 cm and total aperture of 105 cm and (2) a sparse square-shaped full-aspect array. Pilots are extracted from UWB pulses generated as the first derivative of Blackmann Harris (BH) pulse

Table 1. Summary of the Considered MISO Setups

Acronym	TR Technique	Array Configuration	Background
ETRLFS	Equalized TR beamforming	Linear	Free-space
ETRLW	Equalized TR beamforming	Linear	With walls
ETRFAFS	Equalized TR beamforming	Full-aspect	Free-space
ConvLW	Conventional beamforming	Linear	With walls
TRLFS	Conventional TR beamforming	Linear	Free-space
TRLW	Conventional TR beamforming	Linear	With walls
MLFS	TR MUSIC w/o equalization	Linear	Free-space
EMLFS	TR MUSIC w/ equalization	Linear	Free-space
DTRLFS	Differential TR beamforming	Linear	Free-space
DMLFS	Differential TR MUSIC w/o equalization	Linear	Free-space

[*Harris*, 1978] with center frequency of 1.25 GHz and useful bandwidth B covering from DC up to 2.5 GHz. All simulations are carried out using the finite difference time domain (FDTD) method [*Taflove and Hagness*, 2005].

4.2. Spatial Focusing and Temporal Compression

[18] The different setups are summarized in Table 1. Pilots of all setups are normalized to have equal (unity) total energies as follows

$$\mathbf{p}_A(\omega) = \frac{\mathbf{p}_A(\omega)}{\sqrt{\int_\omega \|\mathbf{p}_A(\omega)\|^2 d\omega}} \tag{10}$$

CIR peak values and ISI at the intended receiver and eavesdropper for all setups are plotted in Figure 1 for comparison. To compute the ISI using (2), T is chosen equal to $1/(2B)$. This corresponds to the case of UWB modulation using Nyquist pulses discussed later.

[19] We start with equalized TR beamforming in free-space and use it as a reference for comparison with other setups. Spatial distributions of the peak value of the CIR and the ISI are plotted in Figure 2. It is obvious from the figure that the spatial focusing of this setup is not so good. The power is distributed over a wide region of space, and the eavesdropper (indicated by "x" in the figure) is receiving a significant amount of power. Also, the ISI at the eavesdropper is comparable to that at the receiver. Consequently, the eavesdropper will be receiving a high quality signal that allows it to intercept the signal.

[20] Better spatial focusing is obtained when the same linear array is operating in the presence of rich scattering environment, such as including the surrounding walls shown in Figure 3. This is a result of the way TR exploits multipathing, where frequency components of the CIR add (only) incoherently at all locations in space except at the receiver's location where different frequency components add *coherently* [*Lerosey et al.*, 2004, 2005, 2007; *Derode et al.*, 2003]. This is known as the superresolution property of UWB TR.

[21] It is interesting to observe that, despite the spatial focusing in the presence of walls evident in Figure 3 (higher ratio between CIR peak at the intended receiver compared to other locations), the absolute value of the CIR peak at the receiver is actually less than that in free-space. From the input energy normalization in (10), the

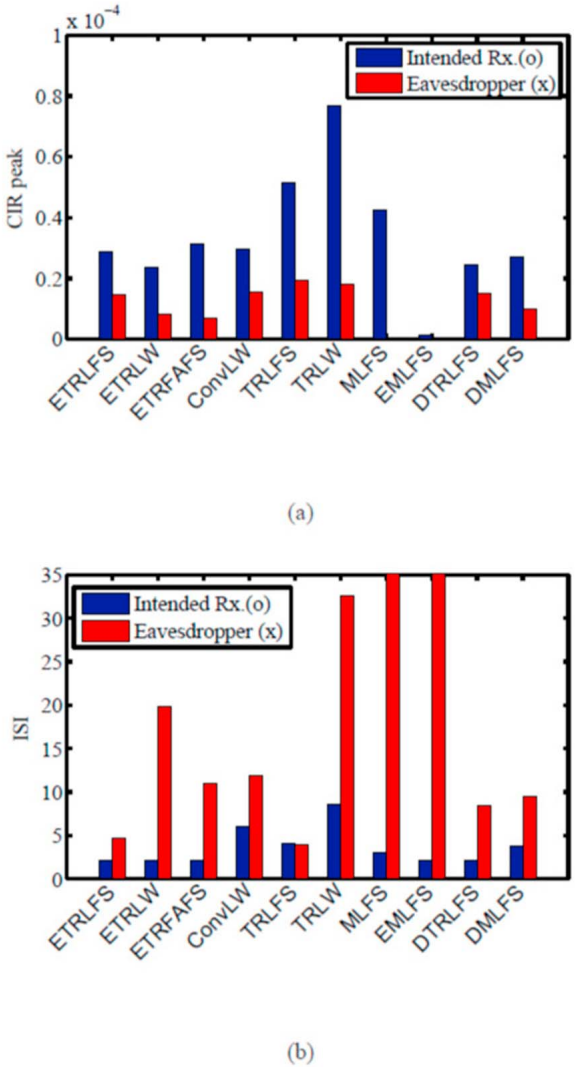

Figure 1. Performance comparison of the proposed MISO setups under equal input power assumption. Acronyms are summarized in Table 1. (a) CIR peak and (b) ISI at the intended receiver and the eavesdropper.

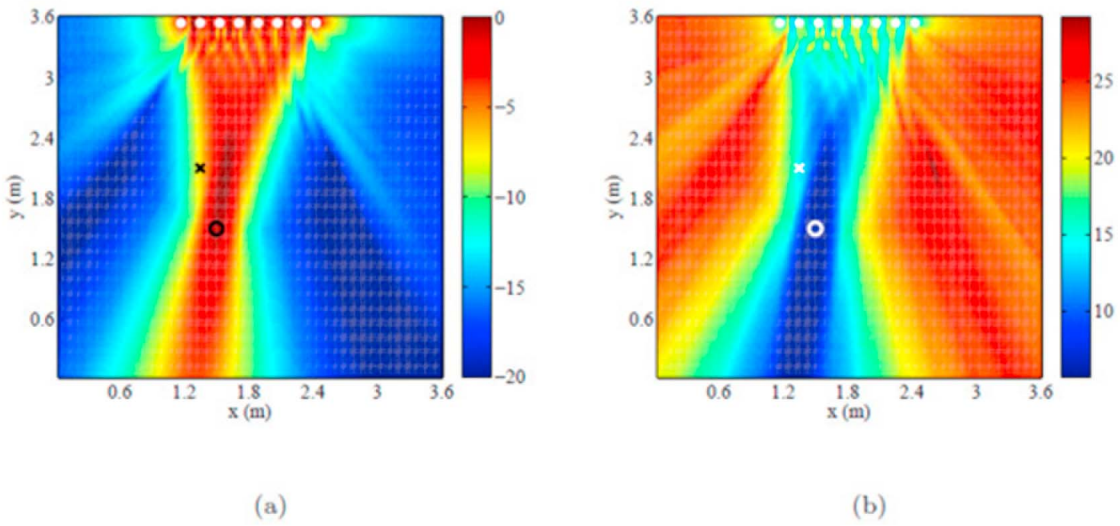

Figure 2. Equalized TR beamforming in free-space using linear array (indicated by white circles). The intended receiver is indicated by "*o*" and the eavesdropper is indicated by "*x*". (a) Normalized CIR peak distribution (in dB). (b) ISI (in dB).

ratio between the CIR peak at the receiver in the presence of walls to that in free-space can be written as $\sqrt{\int_{\omega} 1/\left\|\mathbf{g}_{A,f}(\omega)\right\|^2 d\omega / \int_{\omega} 1/\left\|\mathbf{g}_{A,w}(\omega)\right\|^2 d\omega}$, where subscripts *f* and *w* refer to free-space and walls respectively. This ratio is arbitrary and depends on the scattering medium.

[22] Full-aspect deployment is considered in Figure 4. Such deployment is convenient for indoors communication systems, where fixed transmitters can be mounted on the surrounding walls. Comparing the performance of the full-aspect array with that of linear array with the same number of elements, Figure 4 shows that better spatial and temporal focusing around the receiver are achievable using full-aspect arrays.

[23] Figure 1 shows that conventional (non-equalized) TR provides for higher CIR peaks at the expense of

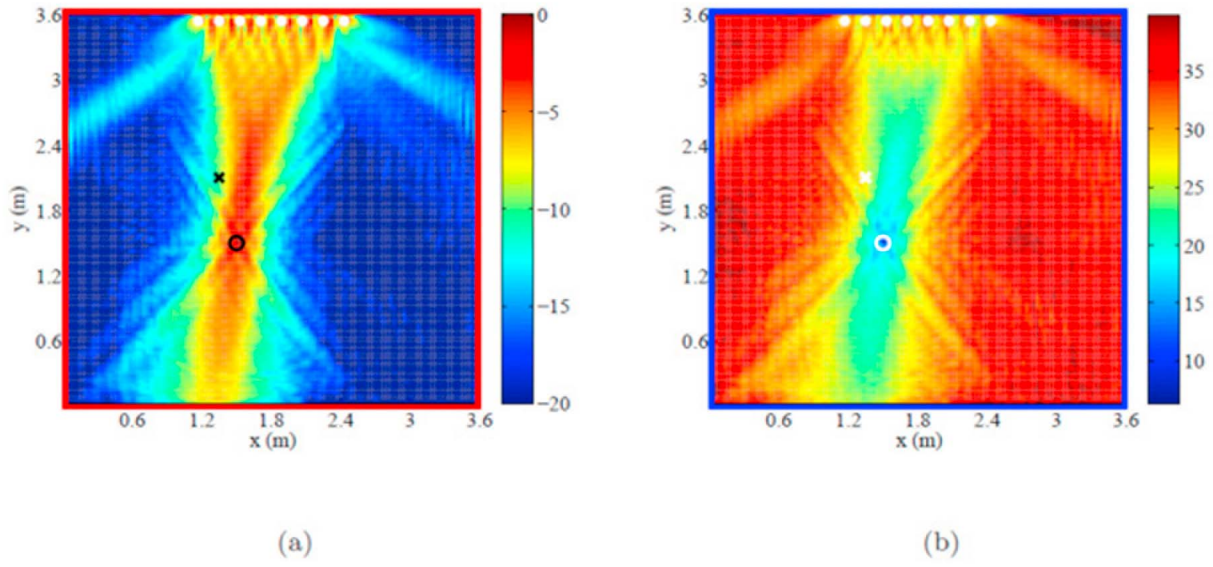

Figure 3. Same as Figure 2, but in the presence of surrounding walls with relative permittivity equal to 4 and thickness equal to 60 cm.

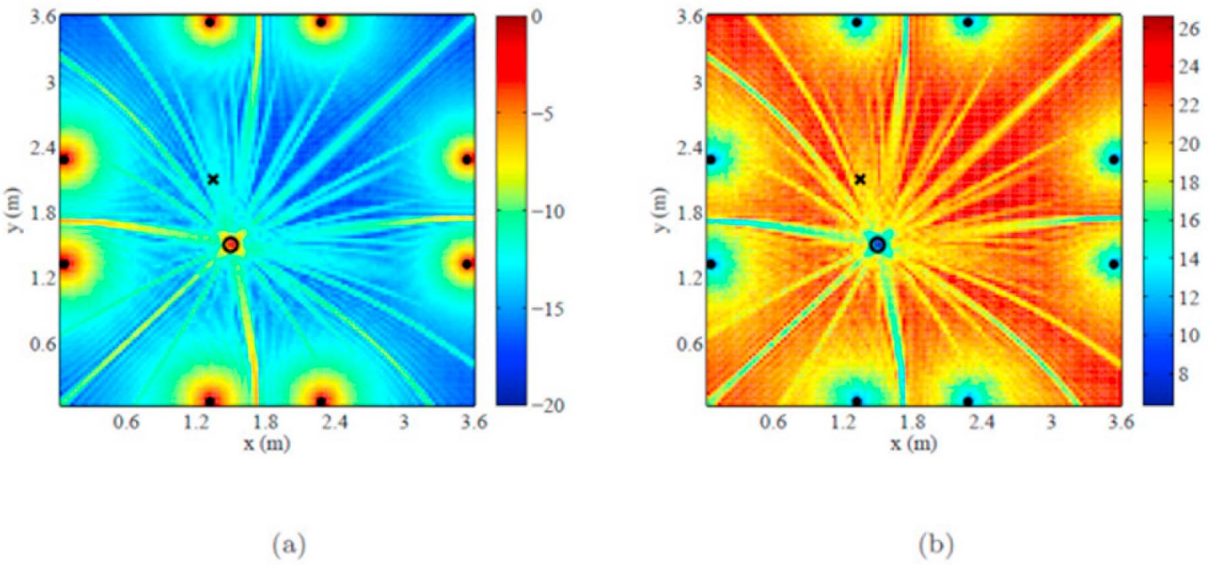

Figure 4. Same as Figure 2 using a full-aspect antenna array.

increased ISI, as compared with equalized TR. For conventional TR, the ratio between the CIR peak in the presence of walls to that in free-space is given by $\sqrt{\int_{\omega} \|\mathbf{g}_{A,w}(\omega)\|^2 d\omega / \int_{\omega} \|\mathbf{g}_{A,f}(\omega)\|^2 d\omega}$, which is always larger than unity. (From physical reasoning, multiple scatterings, such as those offered by walls, confine more energy in the medium and yield longer impulse responses between any transmitter/receiver pair. Therefore the energy of the impulse responses in the presence of walls is larger than that in free-space.) Although multipath serves to increase the CIR peak to temporal sidelobe ratio at the intended receiver [*Lerosey et al.*, 2005], it increases the temporal span of the sidelobes, which increases the overall ISI as shown in Figure 1b [*Edelmann et al.*, 2005].

[24] At this point, it is useful to compare the performance of TR-based beamforming with that of conventional beamforming. Conventional beamforming, despite estimating the receiver's DOA or even its location, is unable to compensate for delays due to multipathing and hence unable to achieve satisfactory equalization. Therefore it yields higher ISI than the equalized TR case as shown in Figure 1b.

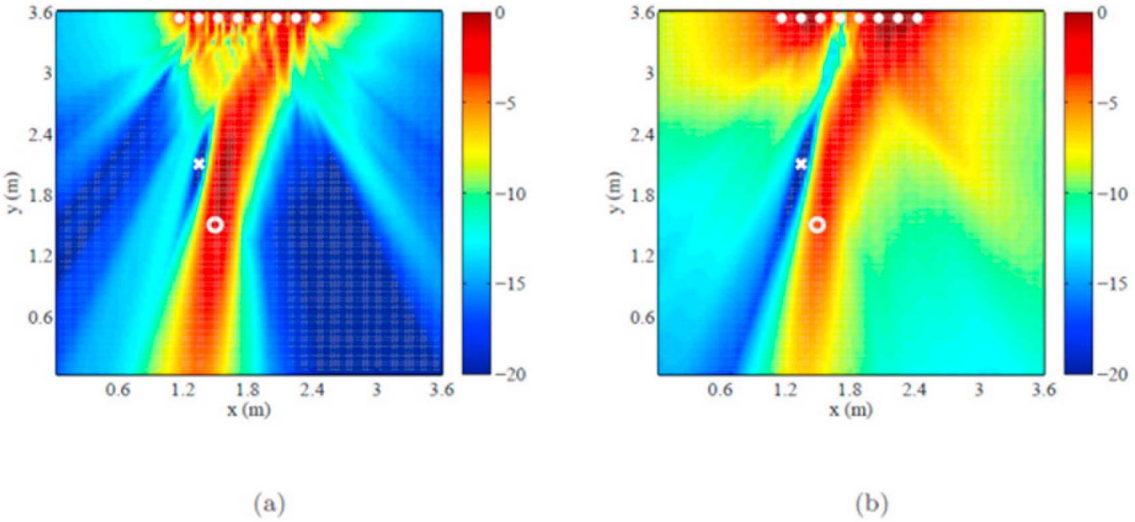

Figure 5. Normalized CIR peak distribution of TR MUSIC using a linear array (a) without equalization and (b) with equalization.

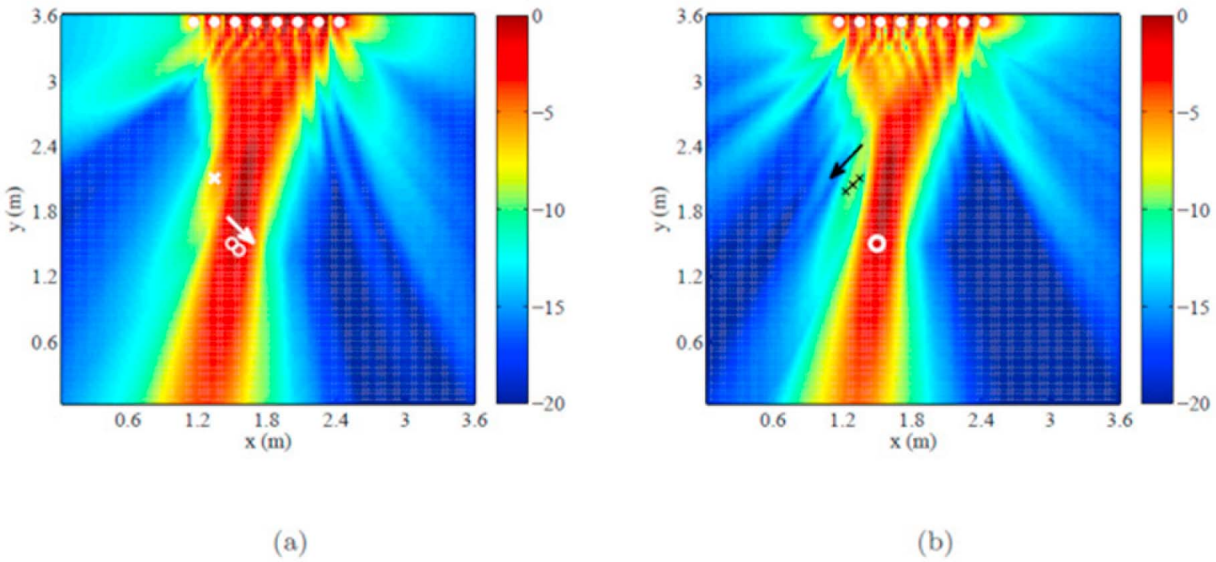

Figure 6. Normalized CIR peak distribution of differential TR in free-space using a linear array. (a) Differential TR beamforming. The intended receiver is moving along the path indicated by the arrow. (b) Differential TR MUSIC. The eavesdropper is moving along the path indicated by the arrow.

[25] The CIR peak images of TR MUSIC without and with equalization for the case of linear array in free-space are shown in Figures 5a and 5b, respectively. It is interesting to compare these images with Figure 2a to see how MUSIC produces null field at the eavesdropper while delivering power to the intended receiver. This is a common feature to both equalized and non-equalized cases. Equalization, however, spreads out the power into larger region of space. This means that, given equal input powers, equalization results in less power reaching the receiver as shown in Figure 1a.

[26] As explained in the previous section, differential TR can be used to extract the pilot signal of passive moving receivers, as that shown in Figure 6a. The resulting CIR peak image is very close to that obtained using TR beamforming in Figure 2a. Differential TR can also be used to extract the steering vectors of moving eavesdroppers to be used in the MUSIC algorithm, as shown in Figure 6b. Note that the null in this case is not perfect because differential TR provides only an approximate version of the steering vector.

4.3. Bit Error Rate Performance

[27] In this section, we compare the bit error rate (BER) performance of the discussed techniques under high and low data rates operations. In the high data rate case, bits are represented by Nyquist pulses whose spectrum covers the entire useful bandwidth of operation (UWB pulses) as shown in Figures 7a and 7b. In this particular example, a maximum bit rate of 5 Gbps is accommodated, which is equal to twice the bandwidth. For the low data rate case, we use binary phase shift keying (BPSK) passband modulation as shown in Figures 7c and 7d. In this example, a bit rate of 0.125 Gbps is used, which corresponds to a −10 dB bandwidth of 0.178 GHz.

[28] Received bit streams at the intended receiver and at the eavesdropper are obtained by convolving the input stream with the corresponding equivalent CIR. Additive white Gaussian noise (AWGN) is added, and the noisy stream is decoded. Assuming perfect synchronization at the decoder, Nyquist pulses stream is decoded by simply sampling the stream at the bit rate, whereas BPSK stream is decoded using coherent detection [*Haykin*, 2001]. Finally, Monte Carlo simulation is used to compute the BER of the decoded stream. For the computed BER to represent a statistically stable measure for the probability of error, the process is repeated over a large number of noise realizations and the results are averaged. In our simulations, we generate streams of 1000 bits and average over 100 noise realizations.

[29] To make comparison easy, considered setups are divided into four groups. The first group includes equalized TR techniques as shown in Figure 8. Note that to provide a consistent measure for comparing different setups, the bit energy E_b in the abscissa of the BER curves represents the pilots energy at the transmitter array (which is equal for all setups) rather than the bit energy at the receiver (which varies from one setup to the other). Since these setups are equalized (have negligible ISI), the BER performance at the receiver depends on the CIR peak value at the receiver. That is why the full-aspect case exhibits better performance. At the eavesdropper, however, the CIR is not perfectly equalized. Therefore, the performance at high data rate is hampered by the internal noise due to ISI, especially for low external noise levels (high E_b/N_0), as evident from the BER saturation in Figure 8b. At low data rates, the effect of ISI is less pronounced, especially in free-space, which allows the eavesdropper to intercept the signal.

[30] The second group compares conventional TR and conventional beamforming with equalized TR as shown in Figure 9. At high data rates, the performance of equalized TR is superior to other techniques. On the contrary, at low data rate the performance is controlled by the power level at

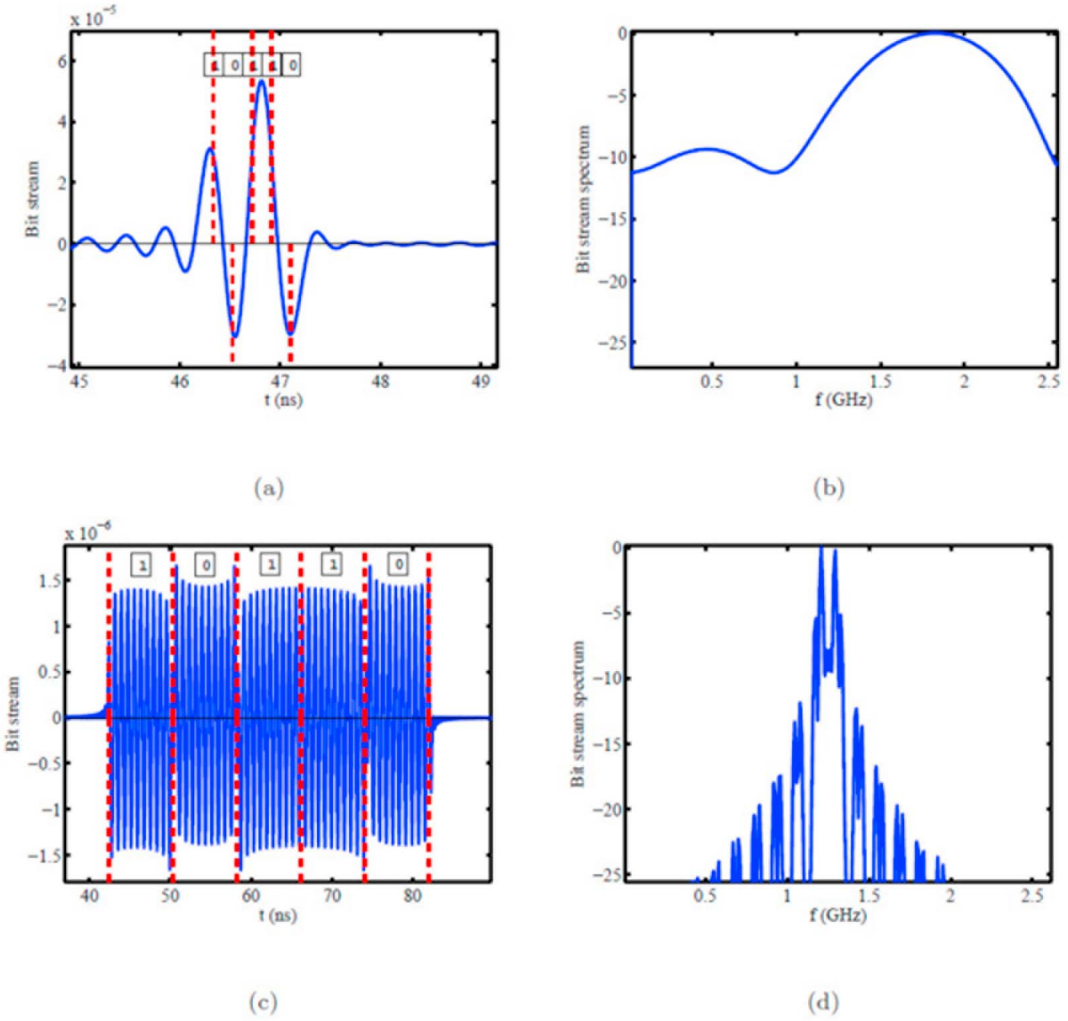

Figure 7. Transmitted bit stream. (a) High data rate time domain signal. (b) High data rate normalized spectrum in (dB). (c) Low data rate time domain signal. (d) Low data rate normalized spectrum in (dB).

the receiver. Therefore, when ISI at the receiver is not the limiting factor, conventional TR operating in rich scattering environments yields the best performance since it provides the highest CIR peak at the receiver and the highest ISI at the eavesdropper.

[31] The third group compares TR beamforming with MUSIC techniques with equalized TR as shown in Figure 10. Using MUSIC significantly increases the BER at the eavesdropper (thus increases covertness) especially at low data rates. However, because of the reduced CIR peak provided by equalized MUSIC, it yields unsatisfactory high BER at the receiver for both high and low rates. Only at very high E_b/N_0 (beyond the limits of Figure 10a), equalized MUSIC performance can outperform that of non-equalized MUSIC, which saturates at high E_b/N_0 due to ISI.

[32] Finally, the fourth group compares differential TR techniques with equalized TR. As shown in Figure 11a and (c), both differential TR techniques yield satisfactory performance at the receiver, comparable with that of equalized TR. At the eavesdropper, differential TR MUSIC serves to increase the covertness by increasing the BER, but with slightly less efficiency than TR MUSIC in Figure 10, as expected.

4.4. Effect of Hardware Limitations

[33] So far, we have studied the performance of different techniques without considering any practical limitations that may be imposed by the utilized hardware. In practice, the time allocated for recording the steering vector of the receiver might not be long enough to capture all multiple scatterings in rich scattering media [*Naqvi et al.*, 2010]. This produces truncated pilots, and therefore imperfectly equalized equivalent CIR. To demonstrate this effect, consider for example the case of equalized TR technique using linear array operating in the presence of surrounding walls. A typical response at the receiver array for a BH pulse derivative transmitted by the receiver in shown in Figure 12a. The recorded signal is truncated at 34 ns which corresponds to 90% of the total energy. The CIRs in the frequency domain for both truncated and full responses are plotted in Figure 12b. Imperfect

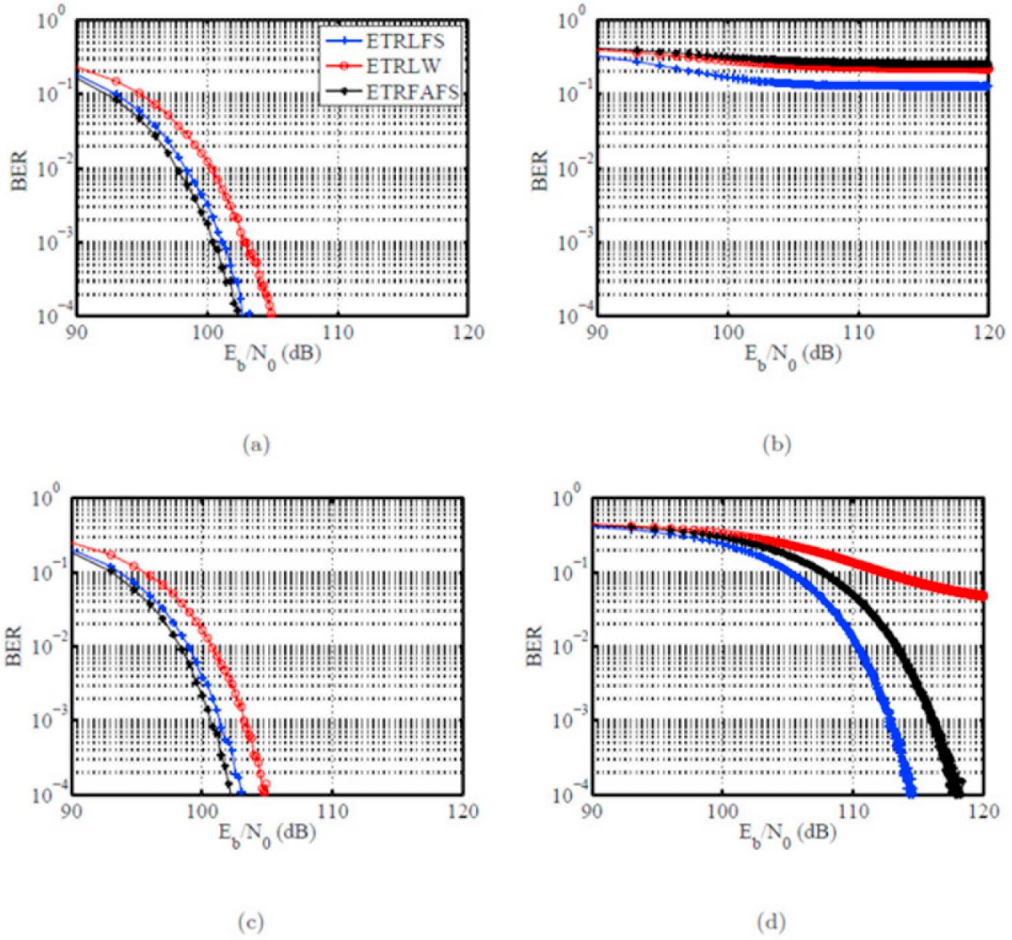

Figure 8. BER performance of equalized TR setups. For high data rate: (a) at the intended receiver, (b) at the eavesdropper. For low data rate: (c) at the intended receiver, (d) at the eavesdropper.

equalization is evident as a result of truncation. This increases the ISI by 100%.

[34] Another limitation may arise from the dynamic range of the array transceivers. Pilots energy distribution among array elements for different setups are plotted in Figure 13. Most techniques result in almost uniform energy distribution among array elements with dynamic range less than 5 dB. Equalized TR MUSIC, however, requires a stringent power distribution with dynamic range of 25 dB. This problem can be mitigated by muting array elements whose energies fall below a certain threshold.

5. Multiuser MIMO Configuration

[35] In multiuser MIMO configurations, the array attempts to communicate with multiple receivers simultaneously. If the interuser interference (IUI) among receivers is adequately mitigated, communication with different users can be achieved in the same time and frequency slots, which is the principle of space division multiplexing. The capacity of the MIMO system is mainly limited by the amount of co-channel interuser interference (IUI) [*Nguyen et al.*, 2005, 2006b; *Wang and Lv*, 2011; *Qiu*, 2006; *Naqvi and Zein*, 2011]. In this section we will show how TR beamforming with MUSIC can be used to mitigate IUI.

[36] Consider the presence of two receivers A and B, the transmitted signal vector in the frequency domain can be written as

$$\mathbf{t}(\omega) = S_A(\omega)\mathbf{p}_A^*(\omega) + S_B(\omega)\mathbf{p}_B^*(\omega) \tag{11}$$

where $S_A(\omega)$ and $S_B(\omega)$ are the information signals to be transmitted to receiver A and B respectively. The received signal at receiver A is given by

$$r_A(t) = s_A(t) *_t h_{AA}(t) + s_B(t) *_t h_{AB}(t) + n(t) \tag{12}$$

where h_{AA} (t) is the CIR of receiver A computed at receiver A, whereas $h_{AB}(t)$ is the CIR of receiver B computed at receiver A. Similarly, the received signal at B can be written as

$$r_B(t) = s_B(t) *_t h_{BB}(t) + s_A(t) *_t h_{BA}(t) + n(t) \tag{13}$$

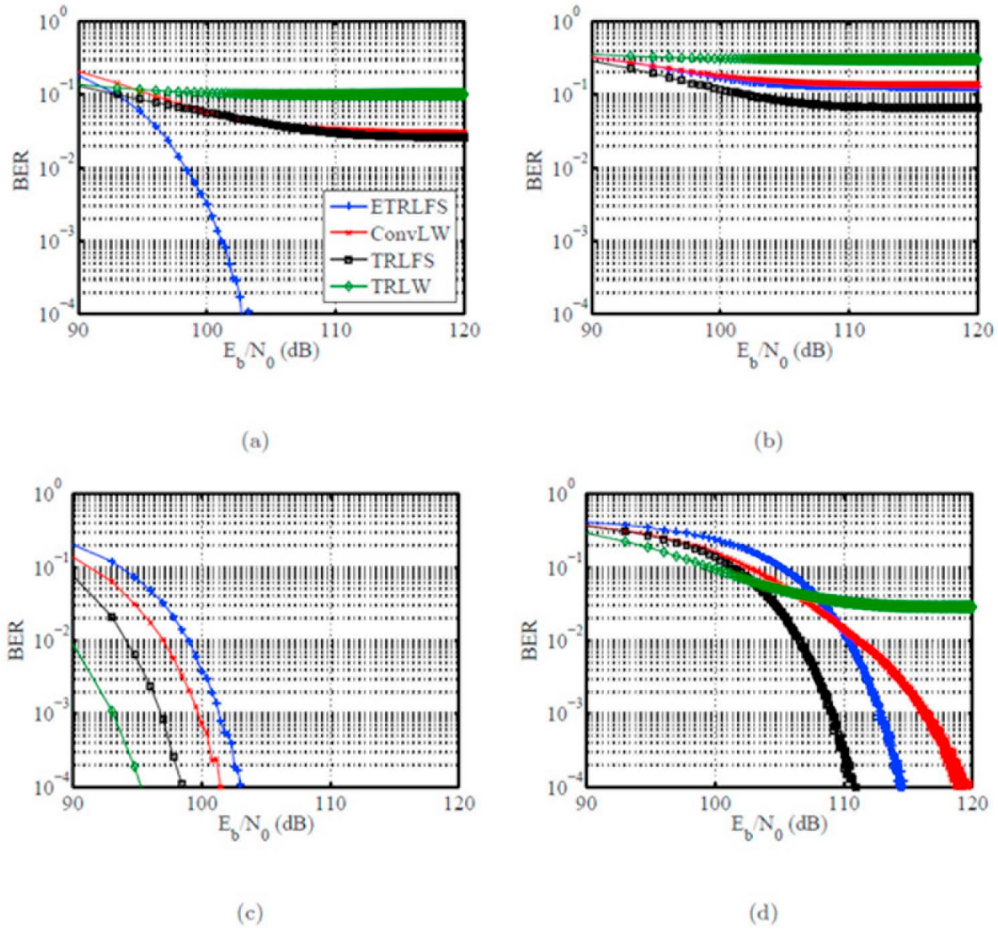

Figure 9. BER performance of conventional beamforming and conventional TR. For high data rate: (a) at the intended receiver, (b) at the eavesdropper. For low data rate: (c) at the intended receiver, (d) at the eavesdropper.

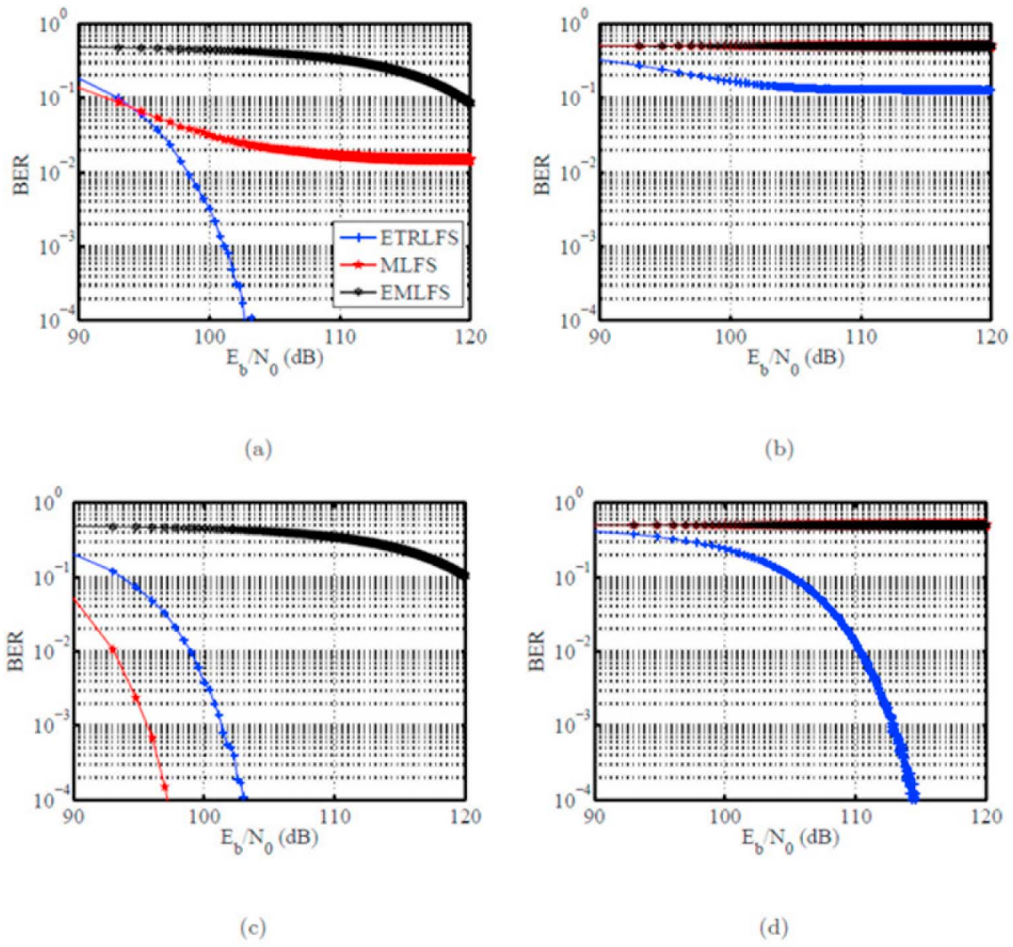

Figure 10. BER performance of TR MUSIC. For high data rate: (a) at the intended receiver, (b) at the eavesdropper. For low data rate: (c) at the intended receiver, (d) at the eavesdropper.

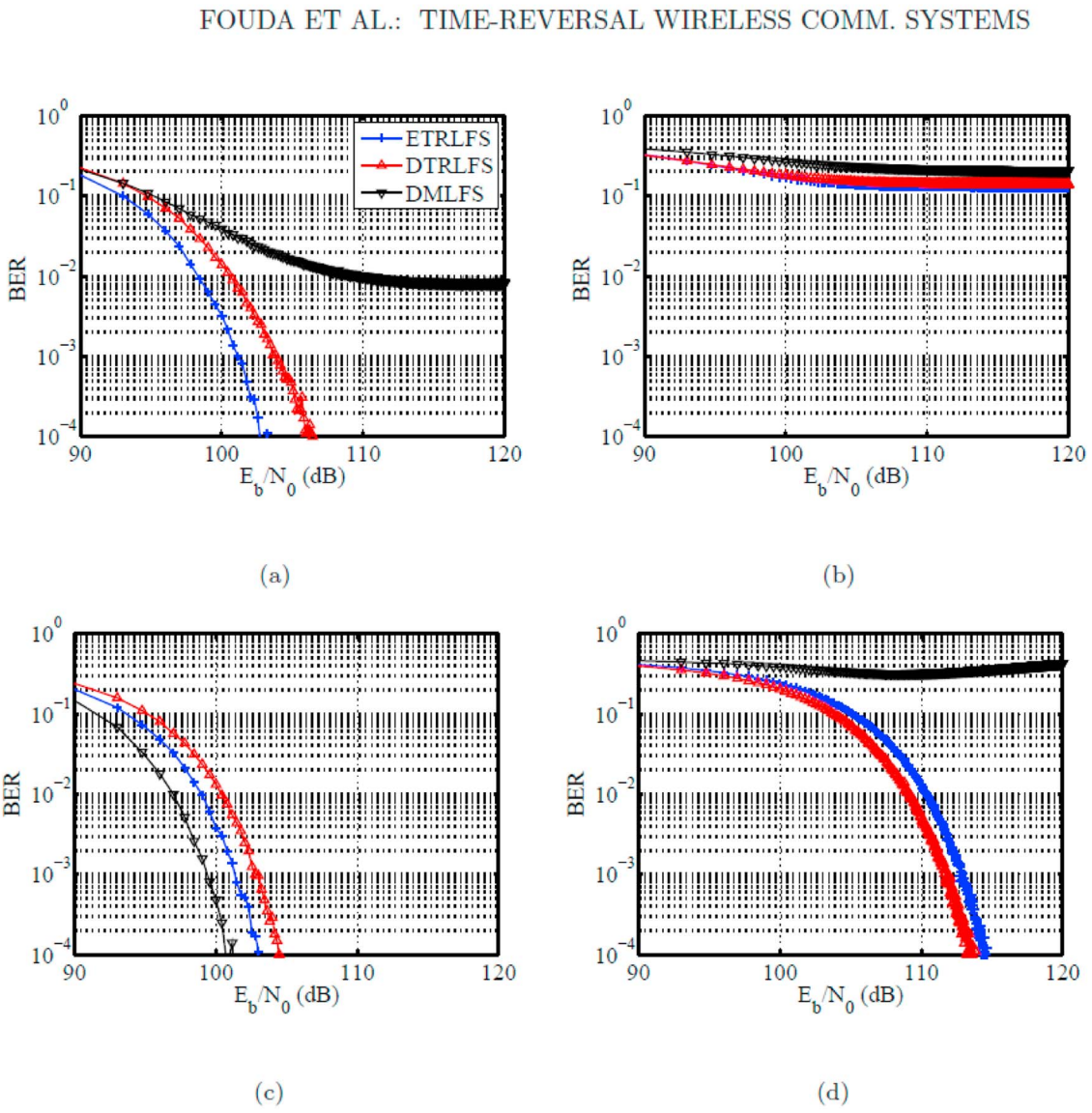

Figure 11. BER performance of differential TR beamforming and MUSIC. For high data rate: (a) at the intended receiver, (b) at the eavesdropper. For low data rate: (c) at the intended receiver, (d) at the eavesdropper.

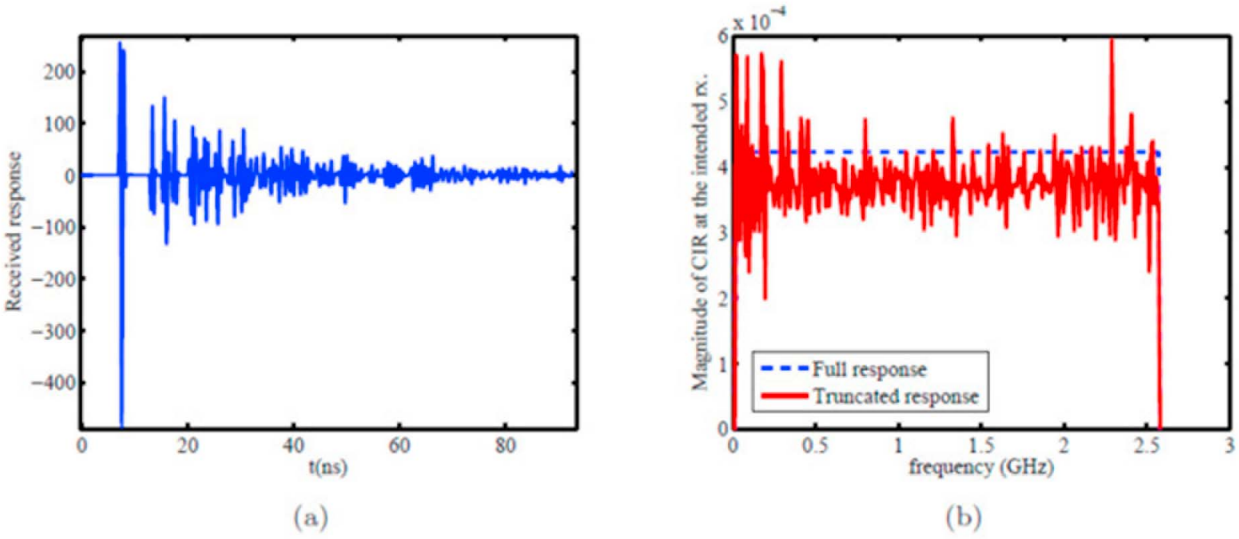

Figure 12. Effect of receiver channel response truncation at the array. (a) A typical response at the receiver array for a BH pulse derivative transmitted by the receiver in the presence of walls. (b) CIR in the frequency domain at the intended receiver.

Obviously, the second terms in the r.h.s. of the above two equations represent undesired interuser interference. TR beamforming with MUSIC can be used to deliver the signal to the intended receiver while imposing null on the other receiver, therefore, it sets the cross terms h_{AB} (t) and h_{BA} (t) to zero, and the self terms become the CIR of the TR with MUSIC technique. As an example, consider the setup in Figure 2, where the eavesdropper now represents receiver *B*. The BER performance of non-equalized TR with MUSIC is compared with that of equalized TR in Figure 14. Note that at high data rate both techniques suffer from saturation with E_b/N_0. Equalized TR saturates because of IUI, whereas TR with MUSIC saturates because of ISI. Nevertheless, TR MUSIC still shows better performance especially at low data rates where IUI is stronger than ISI.

6. Conclusion

[37] We have extended existing TR-based wireless communication strategies by introducing three techniques that satisfy different performance criteria. We have applied them to both MISO and MIMO configurations using both linear and full-aspect arrays. BER performances of different techniques under various operational scenarios were compared for high and low data rates. Two main factors affect the BER: (1) ISI (internal noise) and (2) received power level relative to external noise. Equalized TR beamforming was introduced to eliminate the ISI that limits the performance at high data rates; however, it was shown to possess inferior power focusing compared with conventional TR. Focusing resolution was shown to depend significantly on the array configuration, where full-aspect arrays were capable of providing better focusing than linear arrays. TR beamforming using linear arrays typically does not allow for sufficient degree of covertness, and especially when an eavesdropper is closer to the array than the receiver. In this case, TR beamforming combined with MUSIC becomes very beneficial in producing null field at the eavesdropper location. TR beamforming with MUSIC is also useful in reducing the IUI in MIMO configurations, and therefore increasing the system capacity. In case of passive receivers that can not send pilots, approximate versions of the pilots can be obtained from sequential array acquisitions. Some effects of hardware limitations on the performance, such as truncated impulse response and transmitters dynamic range, were also considered. As for potential future works, we plan to extend these techniques for their applications in dynamically changing and possibly lossy environments. For example, the existence of (lossy) walls further degrades the electromagnetic propagation as well as breaks the TR invariance. Under such conditions, the

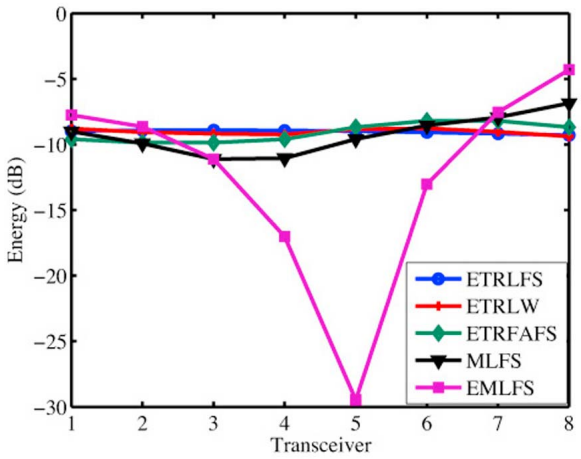

Figure 13. Pilots energy distribution among array elements for different setups.

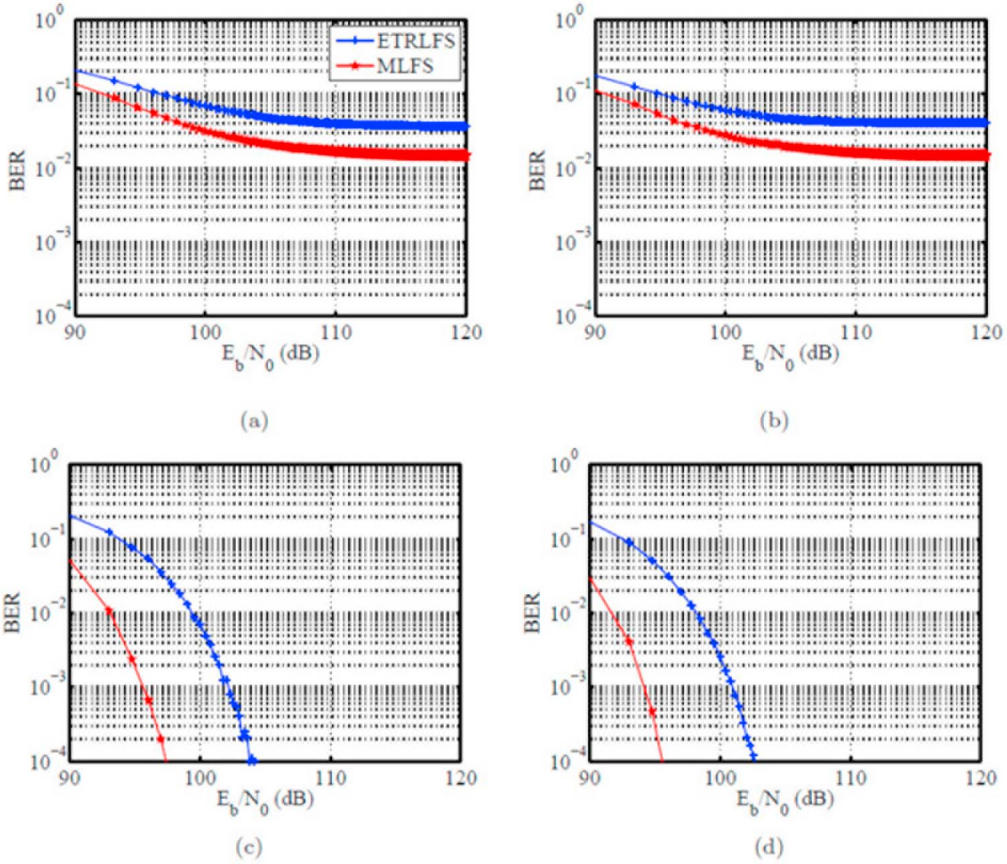

Figure 14. BER performance of MIMO setups. For high data rate: (a) at receiver *A*, (b) at receiver *B*. For low data rate: (c) at receiver *A*, (d) at receiver *B*.

techniques presented here should be appropriately modified to achieve the desired performance.

[38] **Acknowledgments.** This work has been supported by the National Science Foundation (NSF) under grant ECCS-0925272 and by the Ohio Supercomputing Center (OSC) under grant PAS-0110.

References

Blomgren, P., P. Kyritsi, A. D. Kim, and G. Papanicolaou (2008), Spatial focusing and intersymbol interference in multiple-input-single-output time reversal communication systems, *IEEE J. Oceanic Eng.*, *33*, 341–355, doi:10.1109/JOE.2008.925083.

Derode, A., A. Tourin, J. de Rosny, M. Tanter, S. Yon, and M. Fink (2003), Taking advantage of multiple scattering to communicate with time-reversal antennas, *Phys. Rev. Lett.*, *90*, 014301, doi:10.1103/PhysRevLett.90.014301.

Edelmann, G. F., H. C. Song, S. Kim, W. S. Hodgkiss, W. A. Kuperman, and T. Akal (2005), Underwater acoustic communications using time reversal, *IEEE J. Oceanic Eng.*, *30*, 852–864, doi:10.1109/JOE.2005.862137.

Fouda, A. E., and F. L. Teixeira (2012), Imaging and tracking of targets in clutter using differential time-reversal techniques, *Waves Random Complex Media*, *22*, 66–108, doi:10.1080/17455030.2011.557404.

Fouque, J. P., J. Garnier, G. Papanicolaou, and K. Solna (2007), *Wave Propagation and Time Reversal in Randomly Layered Media*, Springer, New York.

Gross, F. (2005), *Smart Antennas for Wireless Communication*, McGraw-Hill, New York.

Guo, N., B. M. Sadler, and R. C. Qiu (2007), Reduced-complexity uwb time-reversal techniques and experimental results, *IEEE Trans. Wirel. Comm.*, *6*, 4221–4226, doi:10.1109/TWC.2007.060251.

Harris, F. J. (1978), On the use of windows for harmonic analysis with the discrete Fourier transform, *Proc. IEEE*, *66*, 51–83, doi:10.1109/PROC.1978.10837.

Haykin, S. (2001), *Communication Systems*, 4th ed., John Wiley, New York.

Jin, Y., J. M. F. Moura, and N. O. Donoughue (2010), Time reversal in multiple-input multiple-output radar, *IEEE J. Sel. Top. Signal Process.*, *4*, 210–225, doi:10.1109/JSTSP.2009.2038983.

Kaiser, T., and F. Zheng (2010), *Ultra Wideband Systems with MIMO*, John Wiley, Chichester, U. K.

Kyritsi, P., G. Papanicolaou, P. Eggers, and A. Oprea (2004), MISO time reversal and delay-spread compression for FWA channels at 5 GHz, *IEEE Antennas Wirel. Propag. Lett.*, *3*, 96–99, doi:10.1109/LAWP.2004.830015.

Lemoult, F., G. Lerosey, J. de Rosny, and M. Fink (2009), Manipulating spatiotemporal degrees of freedom of waves in random media, *Phys. Rev. Lett.*, *103*, 173902, doi:10.1103/PhysRevLett.103.173902.

Lerosey, G., J. de Rosny, A. Tourin, A. Derode, G. Montaldo, and M. Fink (2004), Time reversal of electromagnetic waves, *Phys. Rev. Lett.*, *92*, 193904, doi:10.1103/PhysRevLett.92.193904.

Lerosey, G., J. de Rosny, A. Tourin, A. Derode, G. Montaldo, and M. Fink (2005), Time reversal of electromagnetic waves and telecommunication, *Radio Sci.*, *40*, RS6S12, doi:10.1029/2004RS003193.

Lerosey, G., J. de Rosny, A. Tourin, and M. Fink (2007), Focusing beyond the diffraction limit with far-field time reversal, *Science*, *315*, 1120–1122, doi:10.1126/science.1134824.

Li, D., J. S. Hong, and B. Z. Wang (2009), Improving anti-detection/interception performance for wireless sensor network based on time-reversal technology, in *WiCom '09: 5th International Conference on Wireless Communications, Networking andMobile Computing*, pp. 1–4, IEEE Press, Piscataway, N. J.

Montaldo, G., G. Lerosey, A. Derode, A. Tourin, J. de Rosny, and M. Fink (2004), Telecommunication in a disordered environment with iterative time reversal, *Waves Random Media*, *14*, 287–302, doi:10.1088/0959-7174/14/3/006.

Naqvi, I., and G. E. Zein (2011), Time reversal technique for ultra wide-band and MIMO communication systems, in *Advanced Trends in Wireless Communications*, edited by M. Khatib, pp. 223–240, InTech, New York.

Naqvi, I. H., A. Khaleghi, and G. E. Zein (2010), Time reversal UWB communication system: a novel modulation scheme with experimental validation, *EURASIP J. Wirel. Commun. Netw.*, *2010*, 398401, doi:10.1155/2010/398401.

Nguyen, H. T., J. B. Andersen, and G. F. Pedersen (2005), The potential use of time reversal techniques in multiple element antenna systems, *IEEE Commun. Lett.*, *9*, 40–42, doi:10.1109/LCOMM.2005.01011.

Nguyen, H. T., J. B. Andersen, G. F. Pedersen, P. Kyritsi, and P. C. F. Eggers (2006a), Time reversal in wireless communications: A measurement-based investigation, *IEEE Trans. Wirel. Comm.*, *5*, 2242–2252, doi:10.1109/TWC.2006.1687740.

Nguyen, H. T., I. Kovacs, and P. Eggers (2006b), A time reversal transmission approach for multiuser UWB communications, *IEEE Trans. Antennas Propag.*, *54*, 3216–3224, doi:10.1109/TAP.2006.883959.

Oestges, C., J. Hansen, M. Emami, A. Paulraj, and G. Papanicolaou (2004), Time reversal techniques for broadband wireless communications, paper presented at European Microwave Week 2004, Eur, Microw. Assoc., Amsterdam.

Qiu, R. C. (2006), A theory of time-reversed impulse multiple-input multiple-output (MIMO) for ultra-wideband (UWB) communications, in *Proceedings of the 2006 IEEE International Conference on Ultra-Wideband*, pp. 587–592, IEEE Press, Piscataway, N. J.

Siwiak, K. (2002), Ultra-wide band radio: A new PAN and positioning technology, *IEEE Veh. Technol. Soc. News*, *49*, 4–9.

Taflove, A., and S. Hagness (2005), *Computational Electrodynamics: The Finite-Difference Time-Domain Method*, 3rd ed., Artech House, Norwood, Mass.

Tse, D., and P. Viswanath (2005), *Fundamentals of Wireless Communication*, Cambridge Univ. Press, Cambridge, U. K.

Wang, T., and T. Lv (2011), Canceling interferences for high data rate time reversal MIMO UWB system: A precoding approach, *EURASIP J. Wirel. Commun. Netw.*, *2011*, 959478, doi:10.1155/2011/959478.

Yavuz, M. E., and F. L. Teixeira (2005), A numerical study of time reversed UWB electromagnetic waves in continuous random media, *IEEE Antennas Wirel. Propag. Lett.*, *4*, 43–46, doi:10.1109/LAWP.2005.844117.